UNIVERSITY OF LEEDS

This is a repository copy of *An adaptive finite element procedure for fully-coupled point contact elastohydrodynamic lubrication problems*.

White Rose Research Online URL for this paper:
http://eprints.whiterose.ac.uk/81231/

Article:

Ahmed, S, Goodyer, CE and Jimack, PK (2014) An adaptive finite element procedure for fully-coupled point contact elastohydrodynamic lubrication problems. Computer Methods in Applied Mechanics and Engineering, 282. 1 - 21. ISSN 0045-7825

https://doi.org/10.1016/j.cma.2014.08.026

Reuse

Unless indicated otherwise, fulltext items are protected by copyright with all rights reserved. The copyright exception in section 29 of the Copyright, Designs and Patents Act 1988 allows the making of a single copy solely for the purpose of non-commercial research or private study within the limits of fair dealing. The publisher or other rights-holder may allow further reproduction and re-use of this version - refer to the White Rose Research Online record for this item. Where records identify the publisher as the copyright holder, users can verify any specific terms of use on the publisher's website.

Takedown

If you consider content in White Rose Research Online to be in breach of UK law, please notify us by emailing eprints@whiterose.ac.uk including the URL of the record and the reason for the withdrawal request.

White Rose
university consortium
Universities of Leeds, Sheffield & York

eprints@whiterose.ac.uk
https://eprints.whiterose.ac.uk/

An adaptive finite element procedure for fully-coupled point contact elastohydrodynamic lubrication problems

Sarfraz Ahmed*[1], Christopher E. Goodyer[2], and Peter K. Jimack[3]

[1]*Department of Mathematics, Hazara University, Mansehra, Pakistan*
[2,3]*School of Computing, University of Leeds, UK*

Abstract

This paper presents an automatic locally adaptive finite element solver for the fully-coupled EHL point contact problems. The proposed algorithm uses a posteriori error estimation in the stress in order to control adaptivity in both the elasticity and the lubrication domains. The implementation is based on the fact that the solution of the linear elasticity equation exhibits large variations close to the the fluid domain on which the Reynolds equation is solved. Thus the local refinement in such region not only improves the accuracy of the elastic deformation solution significantly but also yield an improved accuracy in the pressure profile due to increase in the spatial resolution of fluid domain. Thus, the improved traction boundary conditions leads to even better approximation of the elastic deformation. Hence, a simple and an effective way to develop an adaptive procedure for the fully-coupled EHL problem is to apply the local refinement to the linear elasticity mesh. The proposed algorithm also seeks to improve the quality of refined meshes to ensure the best overall accuracy. It is shown that the adaptive procedure effectively refines the elements in the region(s) showing the largest local error in their solution, and reduces the overall error with optimal computational cost for a variety of EHL cases. Specifically, the computational cost of proposed adaptive algorithm is shown to be linear with respect to problem size as the number of refinement levels grows.

KEYWORDS: elastohydrodynamic lubrication; finite element method; linear elasticity; fully coupled approach; adaptive h-refinement; optimization of meshes

1 INTRODUCTION

The use of lubricants between the moving components of mechanical systems helps protect them from direct contact, and therefore reduces both friction and wear. This in turn leads to less energy

*Correspondence to: Sarfraz Ahmed, Department of Mathematics, Hazara University, Mansehra, Pakistan. Email: sarfy001@yahoo.com

consumption and increased life of the machine components respectively. To keep the moving components apart in the presence of a thin lubricant film, a pressure is generated in the film due to the relative motion of the components. Generally, for non-conforming contacts, the pressure generated is very high, which causes a significant elastic deformation in the contact surfaces and hence defines a new shape of the lubricant film. Such a class of problem is known as elastohydrodynamic lubrication (EHL) [1, 2, 13, 18, 42, 43].

The shape of the lubricant film depends upon the geometry of the contacts and the resultant elastic deformation of the contacting surfaces. A most commonly used method to calculate the elastic deformation of the surfaces is based upon evaluation of an elastic deformation integral [13, 19, 29, 42, 43] which is obtained by an analytical solution of the linear elasticity equation on a semi-infinite domain. A number of efficient numerical techniques have been developed over the past few decades using this half-space approach, for example the multilevel multi-integration (MLMI) method [9]. Historically, the most common approaches for discretizing the lubrication equation have been based on finite difference schemes [17, 42]. These methods limit the discretization process to regular structured rectangular meshes using low order approximations, and have been combined effectively with the use of multigrid method [29]. Typically, these difference schemes are loosely coupled with the elastic deformation equation, which allows the efficient combination of multigrid and MLMI [42, 43], but with a slowly converging outer iteration for heavily-loaded cases.

An alternative solution technique is the fully-coupled approach, which consists of solving the discretized elasticity and lubrication equations simultaneously, see for example [25, 33, 34], with the goal of obtaining a faster convergence rate for the iterative solution. These examples are based on the half-space approach for the elastic deflection. The drawback of this approach is that it uses the pressure from all points in the domain to calculate the deflection at each point, which makes the resulting linearized system matrix dense. Furthermore, for heavy loads, the Jacobian matrix becomes almost singular, which makes it hard to reach the solution. A “differential deflection method” was introduced by Evans and Hughes [15, 23, 24, 26]. The advantage of this method is that it uses information from comparatively fewer points in the domain to calculate the elastic deflection at each point. In other words the influence of pressure acting at a point is reduced to a limited locality of that point. Therefore this approach results in a less dense matrix compared to the traditional half-space approach for elastic deflection.

Habchi et al. [20–22] also used a fully-coupled approach to solve the EHL problems. This technique is different however since it replaced the half-space solution method with the direct finite element approximation of the linear elasticity equation on a finite contact domain. The resultant system of discrete equations is therefore very large but is sparse. The author used a sparse direct solver to solve the linearized system at each Newton iteration. Sparse direct solvers are very efficient for small systems but as the resolution and/or the dimension of the problem increases their performance deteriorates and a large amount of memory is required. Recently Ahmed et al. [2, 3] introduced an efficient preconditioned iterative method for such large and highly sparse fully-coupled systems. This solution method leads to substantial savings in memory and time. Most importantly, both the memory and the time growth, with respect to problem size, is shown to be linear. For circular point contact cases, the authors used manually-generated 3D meshes for the linear elasticity approximation, which were based on a large number of experiments in order to obtain a satisfactory EHL solution at the lowest cost as possible. Note that, in the selection of those meshes, smaller mesh spacings were used only in the contact region where the pressure solution exhibits the largest variation [17, 28]. Similarly, the solution of the linear elasticity equation also exhibits large variations close to the contact region. Hence, the mesh elements closest to the contact region are shown to have the largest errors both in the pressure and the linear elasticity solutions [1].

In this paper, the development of an automatic locally adaptive finite element solution scheme for the fully-coupled EHL point contact problems is discussed, which refines the mesh in the contact as well as the elasticity domain based upon local error estimates for the stress. This proposed algorithm therefore combines the several efficiency techniques [2, 38, 48, 49] to obtain performance results that are comparable to those of multigrid and MLMI [42, 43], but with the side effect of predicting the interior deformation and stresses for the contacting elements. It will be shown that the proposed procedure effectively refines the elements in the region(s) showing the largest error in their solution, and reduces the overall error with optimal computational cost. Specifically, the growth in the computational cost of the whole adaptive solution process is shown to be linear with respect to problem size as the number of adaptive levels grows.

2 MATHEMATICAL MODEL AND FULLY-COUPLED APPROACH

2.1 Mathematical model

In this subsection an isothermal EHL point contact model is presented in non-dimensional form. The EHL point contact model considers an equivalent geometry of a contact where contact between two surfaces is represented by an elastic surface and a rigid plane. Note that the equivalent elastic surface contains the total elastic properties of the original contact surfaces, and hence the solution will define the total elastic deformation of both contacting surfaces [2, 21].

2.1.1 Reynolds equation: This governs the pressure distribution through the contact region (Ω_f) for the given geometry and properties of lubricant. It reads (e.g. [1, 43]):

$$\nabla.\left(\epsilon \nabla P\right) - \frac{\partial}{\partial X}\left(\bar{\rho} H\right) = 0, \tag{1}$$

where $\epsilon = \frac{\bar{\rho} H^3}{\bar{\eta}\lambda}$, P and H are the (unknown) dimensionless pressure and film thickness respectively. Also $\bar{\rho} = \bar{\rho}(P)$ and $\bar{\eta} = \bar{\eta}(P)$ are the dimensionless density and viscosity of the lubricant and λ is a dimensionless speed parameter. In this work the Roelands [35] viscosity model and the

Dowson and Higginson [13] density model are used, although the conclusions are not dependent upon these specific choices.

Finally, it is generally assumed that the pressure is equal to the ambient pressure at the boundary of the contact region. Pressure lower than the vapour pressure is physically unacceptable, thus the fluid will cavitate and the pressure will remain equal to the vapour pressure. This process is called cavitation [14, 16, 42]. Since atmospheric and vapour pressure are generally very small compared to the pressure generated inside the contact region they are treated as zero in this model. Hence the pressure throughout the contact is bounded below by zero. Thus, together with the principle of mass conservation [14], the Reynolds boundary conditions reads:

$$P = 0 \;\text{ on }\; \partial\Omega_f \quad \text{and} \quad \nabla P.\vec{n} = 0 \quad \text{at the cavitation boundary,}$$

where $\vec{n}$ is the outward normal vector to the cavitation boundary and $\partial\Omega_f$ is the boundary of computational region. Note that this is a free boundary problem since the location of cavitation boundary is not known prior to computing the pressure solution. Amongst the various possible treatments to handle this free boundary problem (see for example [14, 16, 44]), this work considers a penalty method introduced by Wu [44]. This introduces an additional term (known as the penalty term) for which the modified Reynolds equation reads:

$$\nabla . \left(\epsilon \nabla P\right) - \frac{\partial}{\partial X}\left(\bar{\rho} H\right) - \xi P^{-} = 0, \qquad \text{throughout } \Omega_f, \tag{2}$$

where $P = 0$ on $\partial\Omega_f$, ξ is a suitably large positive number and $P^{-} = \min(P, 0)$. This term has an affect of forcing any negative pressure towards zero, and only dominates in the regions where $P < 0$.

2.1.2 Film thickness equation: This determines the shape of the lubricant film in the contact. For the circular point contact case (with non-dimensional radius of curvature equal to one)

$$H = H_0 + \frac{X^2 + Y^2}{2} + D(X, Y), \tag{3}$$

where H_0 is a central offset film thickness and D is the elastic deformation [1, 21] (see Section 2.2).

2.1.3 Load balance equation: This is a conservation law which ensures that the total pressure generated balances the applied load. For the non-dimensional point contact case this requires [1, 43]:

$$\int_{\Omega_f} P(X, Y) d\Omega_f = \frac{2\pi}{3}. \tag{4}$$

2.2 *Linear elasticity equation:*

In the film thickness equation, the elastic deformation D of the contacting bodies can be modelled by solving Lamé's equation of linear elasticity on a three dimensional domain Ω for point contact problems (e.g. [1, 31], with appropriate boundary conditions):

$$\frac{\partial}{\partial X_j}\left(C_{ijkl}\frac{\partial U_k}{\partial X_l}\right) = 0, \tag{5}$$

where repeated suffices imply summation over the number of space dimensions (three),

$$C_{ijkl} = \lambda\delta_{ij}\delta_{kl} + \mu(\delta_{ik}\delta_{jl} + \delta_{il}\delta_{jk})$$

and λ and μ (known as Lamé's coefficients) are material properties given by

$$\lambda = \frac{\nu E}{(1+\nu)(1-2\nu)}, \qquad \mu = \frac{E}{2(1+\nu)}.$$

Here δ_{ij} is the Kronecker delta, whilst E is the equivalent Young's modulus and ν is the equivalent Poisson ratio of the material used, see [22]. Note that the equation (5) is solved subject to the boundary conditions:

$$\begin{cases} U = 0 & \text{at the bottom boundary } \Omega_D; \\ \sigma_n = n_j C_{ijkl}\frac{\partial U_k}{\partial X_l} = -\delta_{i3}P & \text{at the fluid boundary } \Omega_f; \\ \sigma_n = 0 & \text{elsewhere.} \end{cases} \tag{6}$$

A view of the 3D domain Ω (showing the contact region as a fluid boundary (Ω_f) and the bottom boundary (Ω_D)) is given in the Figure 1. In [21] it is demonstrated that a geometry of size $60 \times 60 \times 60$ is sufficiently large to provide accurate solutions for this non-dimensional model. Hence this elasticity domain is adopted throughout this paper (though a modification of this domain would be of no significance to what follows). Note that $D(X, Y)$ in equation (3) is related to the displacement field $\mathbf{U}$ through the following relation:

$$D = -U_z \mid_{\Omega_f} .$$

2.3 *Fully-coupled approach*

The solution of the EHL point contact problem consists of solving the Reynolds equation (2), the linear elasticity equation (5) and the load balance equation (4). These EHL equations may be discretized using the Galerkin finite element method. However, since the Reynolds equation exhibits an oscillatory behaviour in the pressure solution for heavily-loaded cases (see [29, 43] for example), in order to get a stabilized solution a Streamline Upwind Petrov Galerkin (SUPG) method [11, 45] has been used. The details of our piecewise linear finite element discretization of all the EHL equations can be found in [1–3].

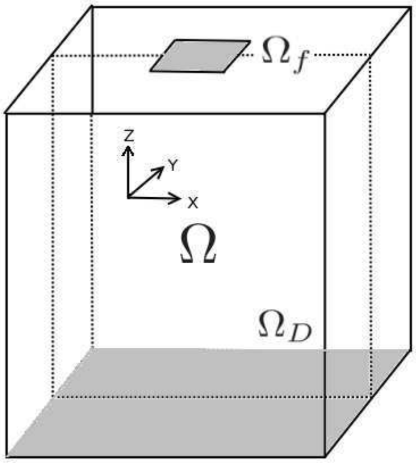

Figure 1: A view of the 3D elasticity domain Ω showing Ω_f (the fluid boundary) and Ω_D (the bottom boundary)

The fully-coupled approach involves the direct coupling of all of the discrete systems arising from the finite element discretization of the EHL equations to form a nonlinear system of algebraic equations for all unknowns (i.e. the 3 elastic displacements at each point in the finite element mesh covering Ω, the pressure approximation at each point in the mesh covering Ω_f and the value of H_0). This monolithic system is solved in one pass using a Newton solver. Typically, such a solver converges for all loadings provided a sufficiently good initial guess is used (see Section 5 for a more detailed discussion of this).

The discrete nonlinear system may be expressed in the following vector form:

$$\begin{cases} \mathbf{R}_P(\mathbf{P},\mathbf{U},H_0) & = \mathbf{0} \\ \mathbf{R}_U(\mathbf{P},\mathbf{U}) & = \mathbf{0} \\ R_{H_0}(\mathbf{P}) & = 0 \quad . \end{cases} \tag{7}$$

Here $\mathbf{R}_P$ represents the system of n_p nonlinear equations arising from the discretization of Reynolds equation, $\mathbf{R}_U$ is the linear system of $3 \times n_u$ equations arising from discretization of the linear elasticity equation and R_{H_0} is the scalar residual of the discretized load balance equation. Similarly, $\mathbf{P}$ is a vector of the n_p unknown pressure coefficients, $\mathbf{U}$ is a vector of the $3 \times n_u$ unknown displacement components and H_0 is the unknown central offset.

When a Newton's method is applied to system (7), the following linear system is obtained at each outer iteration:

$$\begin{bmatrix} \frac{\partial \mathbf{R}_P}{\partial \mathbf{P}} & \frac{\partial \mathbf{R}_P}{\partial \mathbf{U}} & \frac{\partial \mathbf{R}_P}{\partial H_0} \\ \frac{\partial \mathbf{R}_U}{\partial \mathbf{P}} & \frac{\partial \mathbf{R}_U}{\partial \mathbf{U}} & \mathbf{0} \\ \frac{\partial \mathbf{R}_{H_0}}{\partial \mathbf{P}} & \mathbf{0}^T & 0 \end{bmatrix} \begin{bmatrix} \delta \mathbf{P} \\ \delta \mathbf{U} \\ \delta H_0 \end{bmatrix} = \begin{bmatrix} -\mathbf{R}_{\mathbf{P}} \\ -\mathbf{R}_{\mathbf{U}} \\ -R_{H_0} \end{bmatrix} . \tag{8}$$

Starting with an initial estimate for the solution, the Newton procedure consists of solving the linearized system (8) at each Newton iteration and this update is added to the solution obtained at the previous iteration, to provide an improved solution. This process is repeated until convergence is achieved. The details of the solution of the linearized systems (8) are discussed in next section. If the initial guess is not sufficiently accurate then some under-relaxation may be required to achieve the convergence.

3 SOLUTION PROCEDURE

In this section we discuss the overall layout of the new adaptive algorithm used in this work. A suitable initial mesh is first generated using NETGEN [37], where a finer mesh is used in the contact region compared to the other parts of the domain. The selection of a graded initial mesh permits a better starting solution than for a uniform coarse grid however the specific choice for this mesh will be shown to be non-critical for the adaptive procedure. The high-level algorithm used in this work can be split into the following steps.

0. Using the new mesh, build the corresponding data structures for the EHL solver.

1. Set up and solve the fully-coupled EHL problem using the solver described in [2].

2. Estimate the error within each element of the elasticity domain Ω. If the maximum refinement level has been reached or all elements have a sufficiently small error then output is produced and the code exits, otherwise a list of elements is created for refinement.

3. Perform h-refinement. If the mesh optimization option is selected then goto step 4, otherwise goto step 1.

4. Optimize the locally refined mesh. Free up all the previous data structures except for the new mesh and the solution data, and goto step 0.

In the following subsections, a detailed description is provided for each of the above steps involved in the adaptive procedure.

3.1 Solver

The adaptive procedure requires the solution of a nonlinear system (7) following each mesh refinement/generation. As described in the previous section, a Newton procedure is applied to such nonlinear systems, yielding a linear system (8) at each outer iteration. The solution of the system (8) is the most expensive part of each Newton iteration. In this work, a right-preconditioned GMRES method [36] is used to solve (8) at each Newton iteration. The key feature (described in [2]) that makes this approach computationally competitive is the choice of preconditioner, which allows both very fast convergence and a very rapid application at each inner iteration.

This is based upon approximating the $\frac{\partial \mathbf{R}_U}{\partial \mathbf{U}}$ block in (8) by a single algebraic or geometric multigrid V-cycle [8, 10, 39] and using a fast sparse direct solver [12] for the (much smaller) $\frac{\partial \mathbf{R}_P}{\partial \mathbf{P}}$ block of the preconditioner. Results presented in [2] show that this approach substantially outperforms the application of a sparse direct solver to the whole of (8), both in terms of memory and of CPU requirements.

3.2 Error Estimation

Once the fully-coupled system is solved then the error within each element is estimated, using an *'a posteriori'* error estimation. An *'a posteriori'* error assessment is based on the computed numerical solution and is therefore an essential ingredient for any adaptive finite element procedure. Many such estimators have been developed, e.g. [4, 7] and references therein, however this work is based upon the recovery approach first proposed by Zienkiewicz and Zhu [47–49].

3.2.1 An 'a posteriori' error estimate: By way of introduction, let us assume that $\mathbf{u}_h$ is a finite element approximation to an exact solution $\mathbf{u}$ of the linear elasticity equation. Then the error in the computed solution is the difference:

$$\mathbf{e} = \mathbf{u} - \mathbf{u}_h,$$

and the error in their corresponding gradients or stresses, denoted by σ, is:

$$\mathbf{e}_\sigma = \sigma - \sigma_h.$$

For an elasticity problem, stresses are calculated from the finite element solution by:

$$\sigma_h = \mathbf{DSu}_h,$$

where the elasticity matrix $\mathbf{D}$ and the differential operator $\mathbf{S}$ are given by [5] (for the 3D problem):

$$\mathbf{D} = \frac{E}{(1+\nu)(1-2\nu)} \begin{bmatrix} 1-\nu & \nu & \nu & 0 & 0 & 0 \\ \nu & 1-\nu & \nu & 0 & 0 & 0 \\ \nu & \nu & 1-\nu & 0 & 0 & 0 \\ 0 & 0 & 0 & \frac{1-2\nu}{2} & 0 & 0 \\ 0 & 0 & 0 & 0 & \frac{1-2\nu}{2} & 0 \\ 0 & 0 & 0 & 0 & 0 & \frac{1-2\nu}{2} \end{bmatrix}, \quad \mathbf{S} = \begin{bmatrix} \frac{\partial}{\partial x} & 0 & 0 \\ 0 & \frac{\partial}{\partial y} & 0 \\ 0 & 0 & \frac{\partial}{\partial z} \\ \frac{\partial}{\partial y} & \frac{\partial}{\partial x} & 0 \\ 0 & \frac{\partial}{\partial z} & \frac{\partial}{\partial y} \\ \frac{\partial}{\partial z} & 0 & \frac{\partial}{\partial x} \end{bmatrix}.$$

It is now possible to define the corresponding energy norm of the error for this problem, based on the stresses of the solution, via the following expression [47]:

$$\|\mathbf{e}_\sigma\|^2 = \int_\Omega (\sigma - \sigma_h)^T \mathbf{D}^{-1} (\sigma - \sigma_h) \mathrm{d}\Omega.$$

Since neither the exact solution u nor σ are known, a reliable estimator of this error can be obtained if the true gradients σ are replaced with a suitable (higher order) approximation σ^*:

$$\|\mathbf{e}_\sigma^*\|^2 = \int_\Omega (\sigma^* - \sigma_h)^T \mathbf{D}^{-1} (\sigma^* - \sigma_h) \mathrm{d}\Omega \; . \tag{9}$$

Generally the gradients computed from the finite element approximation are discontinuous over the inter-element boundaries. A recovered approximation can be made at each node by averaging the elemental contribution of such gradients over the patch of elements sharing that node. It is then possible to use the linear interpolating polynomials (the same as those used in the finite element approximation) to define a continuous, recovered, approximation over the whole domain. This class of methods are often known as averaging methods [4]. Various estimators can be distinguished based on the specific steps involved in the construction of the average or recovered gradients.

A well-known recovery-based error estimator was proposed by Zienkiewicz and Zhu [47] (known variously as the Zienkiewicz-Zhu or ZZ or Z^2 error estimator). Later on, these authors presented an improved estimator based on superconvergent patch recovery [48, 49]. These estimators are based on the fact that there are points within the elements where the gradients are more accurate and converge to exact values more quickly as the element size decreases. Specifically, such points exhibit superconvergent behaviour in the solution and are therefore referred to as superconvergent points. Thus a more accurate estimate (σ^*) of the true gradient (σ) is recovered at a node by interpolating between the gradients at the superconvergent points in a patch of elements surrounding that node. Nevertheless, the standard ZZ error estimator is both economical and easy to implement, and it has been shown to be just as effective as many residual-based error estimators in different comparative studies, see for example [5–7].

It should be noted that the norm used in (9) is defined over the whole domain Ω. In practice, the squared value of the norm can be obtained by summing up the individual element contributions, i.e.

$$\|\mathbf{e}_\sigma^*\|^2 = \sum_{i=1}^{N} \|\mathbf{e}_\sigma^*\|_i^2, \tag{10}$$

where i is the element number, $\|.\|_i^2$ is defined as in (9) but with Ω replaced the region occupied by element i (Ω_i say) and N is the total number of elements in the current mesh.

Recall that a fully-coupled EHL problem consists of solving the Reynolds equation, the linear elasticity equation and the load balance equation simultaneously. For point contact problems, the linear elasticity equation is numerically solved on a 3D domain Ω, while the Reynolds equation is solved on a 2D fluid domain Ω_f which is a small part of the boundary of Ω. The solution of the linear elasticity equation exhibits large variations close to the fluid region. This tends to lead to the mesh elements close to the fluid region having larger estimated errors. Performing local refinement on these elements therefore improves the accuracy of the elastic deformation solution significantly. An important side-effect however is that refinement of the elements that have a face in Ω_f leads to local refinement of the fluid domain on which the Reynolds equation is solved. Together, the increase in the spatial resolution in Ω_f and the greater accuracy in the computed elastic deformation yield a significantly improved accuracy in the pressure profile. This, in turn, improves the traction boundary condition, to allow an even better approximation of the elastic deformation. Hence, our hypothesis is that a simple and effective way to develop an adaptive procedure for the fully-coupled EHL problem is to apply local refinement to the linear elasticity mesh based upon local error estimation for the elastic stress alone. This hypothesis is explored in sections 4 and 5 below, where its validity is demonstrated.

3.2.2 Refinement strategy: If the global error is already within the prescribed bounds for a given mesh then the goal is already achieved. However, when this is not the case local refinement is necessary in those parts of the domain which exhibit the largest errors. In this work, a tolerance (η_{tol}) is specified for the target relative error (η) in the computed stresses, i.e. :

$$\eta^* = \frac{\|\mathbf{e}^*_\sigma\|}{\|\sigma_h\|} \leq \eta_{tol} \, . \tag{11}$$

The refinement, solution and error estimation steps are repeated until this criterion is satisfied. Unfortunately, it is not always possible to reach the target value (say $\eta_{tol} = 0.05$ [46]) for the error (especially for the 3D problems) due to the availability of computer resources (e.g. memory and CPU cycles). Therefore additional stopping criteria must also be specified, such as maximum refinement levels, minimum element size, memory usage, etc.. In this work, the maximum number of refinement levels are used as a secondary stopping criterion for the adaptive procedure.

As stated earlier, refinement is necessary in the regions of largest error. In other words, one feature of an optimal mesh is that the error is equally distributed among all the elements in the mesh. Mathematically, this may be expressed as [32]:

$$\|\mathbf{e}^*_\sigma\|_i \leq \eta_{tol} \left(\frac{\|\sigma_h\|^2 + \|\mathbf{e}^*_\sigma\|^2}{N} \right)^{\frac{1}{2}} = e_{tol},$$

where i is the element number, N is the total number of elements and e_{tol} (average element error) represents the maximum permissible error for an element. In other words, the ratio:

$$\xi_i = \frac{\|\mathbf{e}^*_\sigma\|_i}{e_{tol}} > 1 \tag{12}$$

specifies the set of elements to be refined. Derefinement is also possible, to save computations, whenever $\xi_i < \xi_{deref} \ll 1$: however this is not considered in this work.

A slightly simpler way of defining e_{tol} in (12) is based upon finding the maximum error over all of the elements (e_{max}) and targeting elements for refinement according to the equation:

$$e_{tol} = ce_{max}. \tag{13}$$

This is the approached used here, where c is a selected constant (if not explicitly stated otherwise, a value of 0.2 is used in this work for demonstration purposes, however a comparison of different values is provided in [1]). Note that any decrease in this parameter may result in flagging quite a lot more elements for refinement and the required goal, of a near-optimal mesh, may not be achieved due to an excessive number of elements being refined at each stage.

3.3 Refinement

Once tetrahedral elements have been marked for refinement this is then implemented using the TETRAD software [38]. The algorithm used in TETRAD is hierarchical in nature and is suitable for both mesh refinement and derefinement processes.

Only the mesh refinement routines are used here, based upon all edges of all of the marked elements being tagged for refinement into two. If an edge is marked for refinement then it leads to refinement of all elements sharing that edge. The refinement process takes into account only two types of subdivision. A regular subdivision in which each parent element is divided into eight child elements by introducing new nodes bisecting each edge. In the first instance this leads to removal of four corners leaving an octahedron behind. The division of this octahedron further results into four new child elements on the basis of dissection by the longest diagonal [27, 38]. The other kind of subdivision, the so-called green refinement, takes place where not all of the edges of an element are marked for refinement, and this avoids the possibility of introducing “hanging nodes” (nodes on edges which are not the vertices of all elements sharing those edges) without introducing any additional edge refinement. Note that green refinement often leads to poor quality elements, and therefore a precaution is taken into account in the development of TETRAD that a green element may not be refined further. In such a case, the previous green refinement of the parent element is replaced with regular refinement. Thus the green refinement always appears at the interface between lower and higher grid levels. As a consequence, the poor quality elements never appear in the region of interest provided appropriate flagging criteria have been used for adaption. Finally, it should be noted that the scaling of the fundamental refinement process is close to optimal linear behaviour [38] and is not significantly affected by the mesh depth.

3.4 Optimization of Meshes

In [1], it is observed that the unstructured meshes resulting from hierarchical mesh refinement often lead to poor quality EHL results without appropriate mesh optimization. In other words, the accuracy of the EHL solution can be improved by optimizing the quality of mesh prior to any computation. In this work, this fact is also taken into account for the meshes resulting from the local refinement process.

In order to combine optimization with local mesh refinement, the meshes obtained once the refinement is performed are passed to NETGEN [37], where a smoothing process is performed via edge and face swaps, local node movement, and some collapsing of elements. Note that, unlike [30], the optimization does not seek to reduce the error further, rather it is undertaken to ensure minimization of a quality functional which quantifies the quality of the mesh. An advantageous side-effect of the optimization is that the collapsing of elements in the optimization process also leads to a small reduction in the size of problem compared to the original mesh. A difficulty encountered with this approach is how to handle transfer of the solution data between the grids before and after smoothing. Furthermore, the optimization processes destroys the mesh hierarchy, so that neither de-refinement nor the use of geometric multigrid preconditioning is easily possible.

Smoothing via NETGEN [37] also has the feature that the mesh optimization only takes place in the interior of the domain, i.e. the surface mesh remains unchanged. The advantage of this is that the latest estimate of the pressure solution can be transferred to the new optimized mesh without any difficulty. However, to produce an initial guess for the elasticity solution on this changed mesh, one needs to solve the elasticity equation corresponding to the surface pressure. Hence, at the cost of a solution of the elasticity equation (equivalent to less than the cost of one fully-coupled Newton iteration) one obtains a consistent initial guess from which the fully-coupled iteration converges very quickly. Note however that the next refinement of green 2D elements on the fixed surface mesh will lead to even more poor quality surface mesh elements, regardless of an optimized 3D mesh. The poor quality surface mesh in the fluid region may affect the accuracy of the pressure solution. One possibility to avoid the low quality surface mesh is to perform the mesh optimization only at the final level of the mesh hierarchy, to improve the accuracy of the final solution. This is therefore considered as one of the possible strategies in this work.

4 EHL RESULTS

Recall from the previous section that the post processing (smoothing) of the adapted mesh has the potential to improve the accuracy of the computed solution on that mesh. Note however that if the optimization is performed then it destroys the mesh hierarchy. Moreover, optimizing the meshes at each refinement level may result in a poor quality surface mesh after a number of refinement levels since any green refinement at the surface remains. This, in turn, may affect the accuracy of the solution of the Reynolds equation. To assess the accuracy of the solution procedure three different possibilities are therefore considered, which ultimately lead to three variants of the main algorithm (see the start of Section 3).

- The first variant of the solver skips step 4 and repeats from step 1 until the stopping cri-

Table 1: Non-dimensional parameters for the contact between steel surfaces [42].

Parameters	Values
Moes parameter, L	10
Moes parameter, M	20
Maximum Hertzian pressure, p_h	0.45GPa
Viscosity index, α	2.2×10^{-8}Pa^{-1}
Viscosity at ambient pressure, η_0	0.04 Pa s
Total speed, u_s	$1.6\ \mathrm{m\,s^{-1}}$

terion is reached. In this case TETRAD keeps a record of all of the refinement history and therefore green elements are prevented from further refinement (and the use of the geometric multigrid preconditioner is possible too, though not implemented here) and the initial guess at each stage is a simple interpolant from the previous solution.

- The second variant of the main solver utilizes step 4 at each refinement level and therefore repeats the process from step 0 with the new mesh. Since the surface mesh, and hence the 2D fluid mesh, does not change, so the solution of the Reynolds equation is transferred to this new mesh without any difficulty, and solving the elasticity equation yields an initial guess for the displacement using this new mesh. Hence, an overall improved initial guess leads to fewer Newton iterations to achieve convergence of the fully-coupled system. However, the quality of the surface mesh may deteriorate with each additional local refinement.

- To avoid the risk of successive green refinement at the surface mesh, the third variant only utilizes step 4 at the final level of refinement, and hence a surface mesh is obtained with a relatively good quality.

Having defined the different variants of the adaptive algorithm, a comparison is made between their accuracy and performance for a typical EHL problem. The test case considered in this section is taken from [42] and given in Table 1. In the calculations, two different initial coarse meshes are used. There is no specific reason in the choice of these initial meshes other than to produce a relatively good starting solution and allow the sensitivity to the choice of initial mesh to be considered. The first initial mesh is composed of a total of 16671 points where 487 of them lie on the surface common to the fluid domain. This means that this initial mesh is relatively fine close to the contact region compared to the remaining region of the elasticity domain. In the second choice of an initial mesh, relatively small mesh sizes are used yielding a mesh with 22234 points in total, of them 691 points are in the fluid region.

4.1 Implementation of Error Estimator

Using initial mesh with 16671 mesh points (for demonstration purposes), Figure 2 shows a cut through the centreline of the 3D domain after different iterations of h-refinement based adaptivity. The elements are coloured using their element sizes. Hence the elements with very small

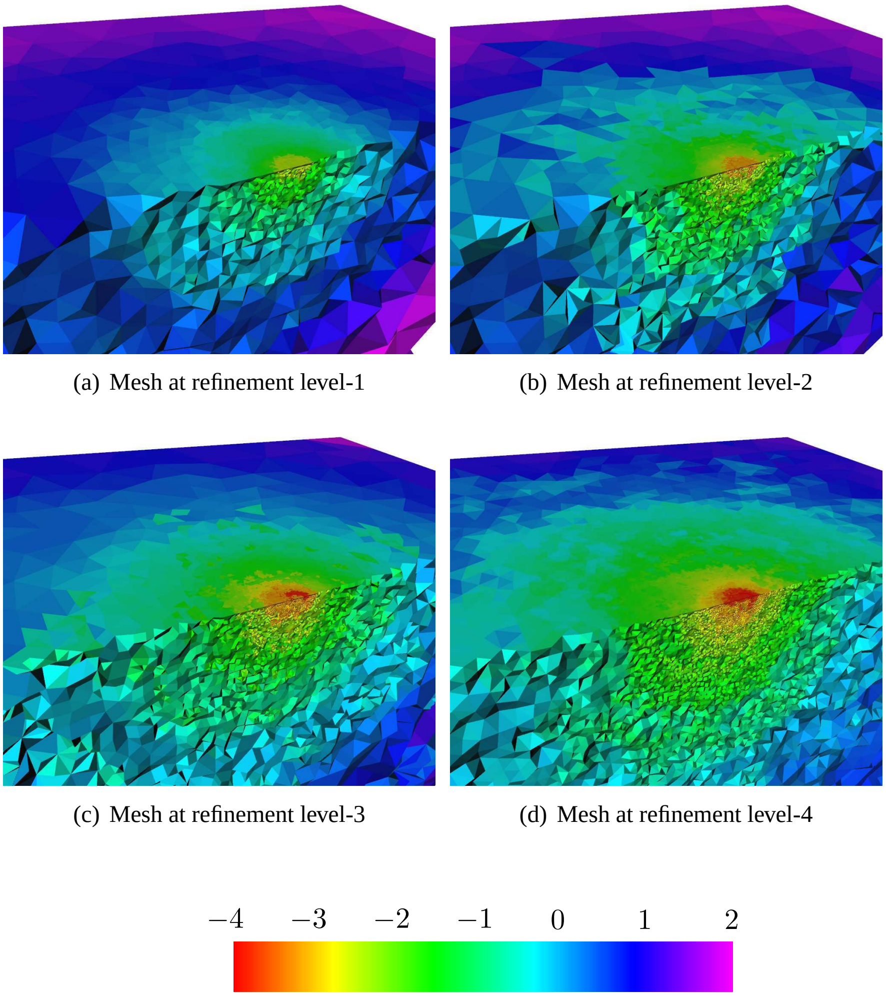

(a) Mesh at refinement level-1

(b) Mesh at refinement level-2

(c) Mesh at refinement level-3

(d) Mesh at refinement level-4

(e) Color scheme used for different values of $\ln$(element size).

Figure 2: A view of meshes at different refinement levels based upon an initial mesh with 16671 points.

mesh sizes ($h_e \approx e^{-4}$) are shown by red and those with large ($h_e \approx e^2$) are shown by purple. One can see that the local refinement is targeting mainly those parts of the domain close to the contact region. However, as the refinement levels go up, the refinement also extends to the parts of the domain away from the fluid region. Moreover, Figure 2(c) shows an arc-shaped region (corresponding to the pressure-ridge region that is present in a typical EHL solution, see Figure 3) of the most highly-refined elements. This indicates that this is a region where the pressure-ridge affects the elastic deformation solution more significantly. Overall, this experiment (and others reported below and in [1]) suggests that our hypothesis, that the proposed error estimation and refinement strategy is effective for fully-coupled EHL problems, does indeed hold. In particular,

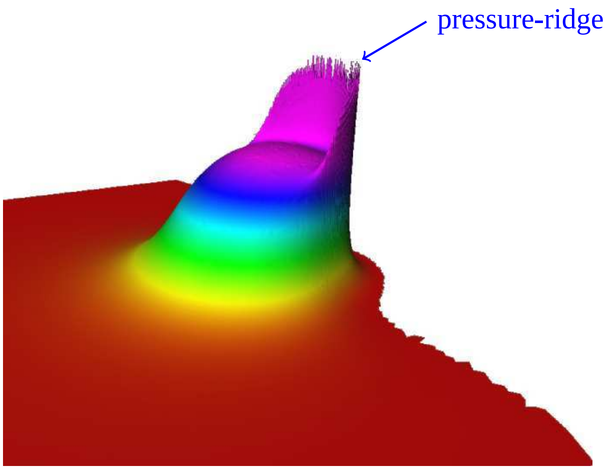

Figure 3: A typical EHL solution - note the typical pressure-ridge which occurs on the outflow side of the contact.

the corresponding 2D mesh for the Reynolds equation is getting finer in the region where, qualitatively, it may be expected. A more quantitative assessment of this follows in the next subsection (along with a comparison of different initial meshes).

4.2 Accuracy Appraisal

In this subsection, an accuracy appraisal of the different variants of the solver is considered. As a first case, the initial mesh with 16671 mesh points is used as the base level mesh. The EHL problem is set up and solved on this starting mesh. Once the solution is obtained, local error estimation on each element of the mesh is made according to equation (9) (but with Ω replaced the region occupied by element i i.e. Ω_i), while a global error estimation is obtained according to equation (10). Having the local error estimate for each element in hand, a set of elements are marked for refinement according to equation (13). As soon as the refinement is performed, the procedure is repeated again until the maximum number of levels specified are reached (for testing purposes the maximum refinement level is used here as stopping criterion). Recall that variant 2 of the solver also performs an optimization process on the refined meshes at each refinement level while variant 3 applies the optimization process only at the last refinement level.

For the different mesh refinement strategies, Table 2 shows a comparison of their behaviour in terms of problem size (both in the pressure unknowns and total problem sizes) and the solution properties (in terms of central and minimum film thicknesses). In the case of uniform (global) refinement (optimized and non-optimized), the pressure unknowns are increasing by about a factor of four, and the total problem size by a factor of about eight, at each level. On the other hand the local refinement process targets elements for refinement so the problem sizes grow more slowly. Note that in each case the local refinement mostly affects the elements close to the contact region (see, also Figure 2). It can be seen that as the local refinement level goes

Table 2: Statistics for solutions using uniform refinement and adaptive h-refinement. Variant 1 performs no mesh optimization, variant 2 performs optimization at every level, and variant 3 performs optimization at the finest level only.

level	uniform refinement		h-refinement		
	non-opt	opt.	variant 1	variant 2	variant 3
number of pressure unknowns n_p					
0	431	431	431	431	431
1	1777	1777	897	897	897
2	7217	7217	3357	3489	3357
3	-	-	8679	7477	8679
4	-	-	16874	19231	16874
Total degrees of freedom					
0	50043	50043	50043	50043	50043
1	381809	354230	66136	61210	66136
2	2994948	2704035	385831	279022	385831
3	-	-	1122655	639962	1122655
4	-	-	3739788	3011678	2827140
central film thickness H_c					
0	0.39677	0.39677	0.39677	0.39677	0.39677
1	0.42500	0.42446	0.40666	0.40644	0.40666
2	0.43071	0.43002	0.42479	0.42482	0.42479
3	-	-	0.42931	0.42829	0.42931
4	-	-	0.43025	0.43024	0.43027
minimum film thickness H_m					
0	0.26047	0.26047	0.26047	0.26047	0.26047
1	0.28472	0.28442	0.27163	0.27208	0.27163
2	0.29051	0.29112	0.28715	0.28744	0.28715
3	-	-	0.29034	0.28947	0.29034
4	-	-	0.29133	0.29121	0.29129

up the difference between the computed solution to that of uniform refinement cases becomes smaller. For example, variant 1 results in approximately the same solution after two levels of refinement with a much smaller problem size compared to that with the uniform refinement cases. Variant 2, which optimizes the meshes at every refinement level, seems to yield the same accuracy in results as variant 1, but with a relatively smaller problem size. Note that it was not possible to perform a third level of uniform refinement (with or without optimization) due to unavailability of computing resources as one can see that this would lead to a very large problem size.

It should be noted that the output of variant 3 differs from variant 1 only at the finest level due to the additional optimization process. This optimization process leads to a significant decrease in the total size of the finest level problems while ensuring the overall accuracy of the solution. In other words variant 3 yields the same accuracy in the solution (compared to variant 1) with a smaller problem size at the finest level. Overall, it appears that the computed values of both H_c and H_m are converging approximately quadratically with each mesh refinement, and that this observation holds for each variant. Furthermore the results suggest that variants 2 & 3 end up with the same accuracy in their solution with relatively small problem sizes compared to variant 1. Indeed, we shall see next that both variants 2 & 3 result in better accuracy per degree of freedom than both variant 1 and the uniform refinement cases.

A comparison of the estimated global errors obtained for each variant of the solver is shown

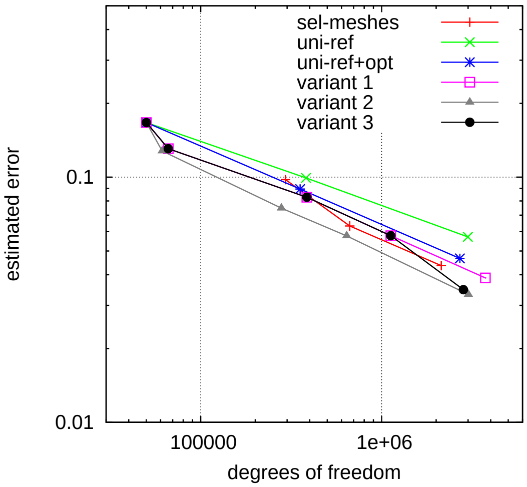

(a) $e_{tol} = 0.2e_{max}$

Figure 4: A comparison of global error estimation using a coarsest mesh of 16671 points.

in Figure 4. Note that the global error estimation is for the stress, with a converging pressure profile (different for each mesh strategy) as the traction boundary condition. The cases of uniform refinement (with and without optimization) along with the hand-tuned mesh cases (denoted “sel-meshes”) [3] are also included. One can see that a non-optimized uniform refinement process leads to small reduction in the (estimated) error with increasing problem size. However, if the meshes are optimized after each uniform refinement step then an improved rate of reduction in the error is obtained. In this example, the local refinement cases (all three variants) appear to have a superior error reduction rate, with respect to problem size, as compared to both cases of uniform refinement. It can be seen that optimization of meshes at each refinement level further improves the rate of error reduction with respect to the problem size. It should also be noted that the last level optimization (variant 3) significantly reduces the error at the finest level, and results in approximately the same accuracy as that obtained with the use of optimization at every level (variant 2). Finally, the hand-tuned mesh cases perform better than the local refinement without post-optimization of meshes (variant 1) however the automatic adaptivity with mesh smoothing does better still.

As a second test case, a different initial mesh composed of 22234 mesh points is considered. Figure 5 shows the accuracy appraisal for different variants of the solver compared to the use of uniform refinement and the hand-tuned mesh cases. The same behaviour in the results can be observed as before, however the case of optimized uniform refinement is now competitive with the error reduction rate for the non-optimized local refinement. Nevertheless, it can again be seen that the local refinement cases (both with optimization at only the last or at every level, variants 3 & 2 respectively) perform better than the other cases in terms of accuracy per degree of freedom.

As a whole, one can conclude from these experiments that the local refinement of meshes with

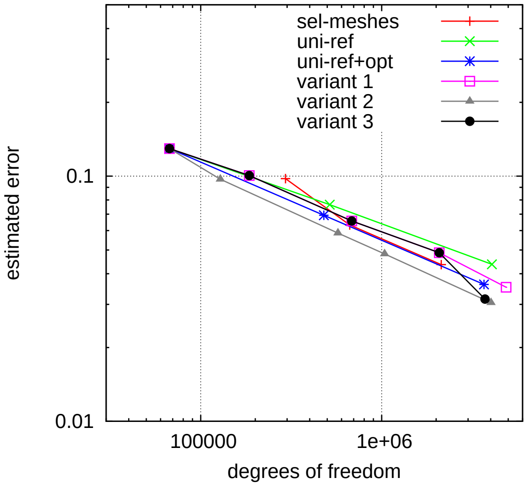

(a) $e_{tol} = 0.2e_{max}$

Figure 5: A comparison of global error estimation using a coarsest mesh of 22234 points.

post optimization at only the final, or at all levels, results in more accurate results per degree of freedom. Most importantly, the adaptive algorithm (with at least final level optimization) leads to better results compared to the hand-tuned mesh cases. Indeed, the use of automatic mesh refinement based upon '*a posteriori*' error estimation has clearly led to better meshes than the hand-tuning approach described in [3].

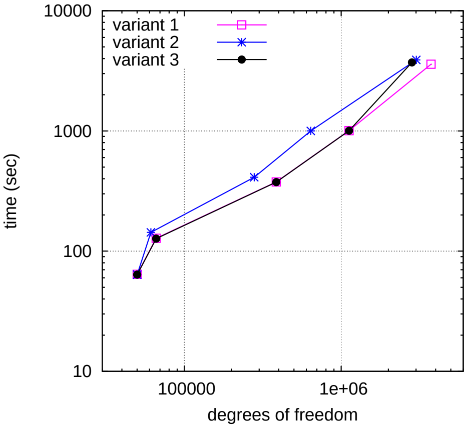

(a) $e_{tol} = 0.2e_{max}$

Figure 6: A comparison of performance of different variants of adaptive finite element solver using the coarser initial mesh.

Table 3: Statistics of solution at different refinement levels. Variant 1 performs no optimization, variant 2 perform optimization at every level, and variant 3 performs optimization at the finest level only.

level	uniform refinement		h-refinement		
	non-opt.	opt.	variant 1	variant 2	variant 3
Total nonlinear iterations					
0	14	14	14	14	14
1	9	9	10	9	10
2	4	4	5	4	5
3	-	-	4	3	4
4	-	-	5	3	3
Average number of linear iterations per one nonlinear iteration					
0	11.4	11.4	11.4	11.4	11.4
1	12	11	11.8	11.1	11.8
2	13.3	13	15.0	13.5	15.0
3	-	-	15.0	12.7	15.0
4	-	-	15.0	11.0	11.3

4.3 Performance

In this subsection, the CPU timings of the different variants of the proposed adaptive finite element solver are assessed. For the initial mesh case 1, the computational times are plotted in Figure 6. Here, an initial jump in the computational time can be observed while switching from the base level to the first level. The reason is that the first refinement process led to refinement of only a few elements meaning that the refinement overhead was relatively large (see Section 4.5 for further details). Moreover, variant 2 applies an optimization process on the refined mesh which leads to a slightly smaller problem size but the total time has increased compared to other two variants. After the first level, the growth in the time is almost linear (i.e. $\mathcal{O}(N)$) for each of the variants, however variant 3 shows a jump in the computational time on the final level due to the optimization process on this last level mesh. Overall, the optimization of the refined meshes, at least at the final level, leads to a relatively small change in computational time (but to relatively more accurate results, as discussed above).

Table 3 gives statistics of average number of linear iterations and the number of nonlinear iterations for each variant of the adaptive solver. It can be seen that as the refinement level increases in each case, fewer nonlinear iterations are required to achieve convergence because of the availability of the good initial guess based upon solution at the previous level. Importantly, the performance of the solver seems independent of the adaptivity method used. Moreover, the optimization of meshes at final level in variant 3 results in a relatively small number of nonlinear iterations compared to variant 1. Similarly, variant 2 requires even fewer nonlinear iterations at the intermediate levels. In addition to nonlinear iterations, variant 3 requires fewer linear iterations per nonlinear iterations at the final level while this number is also reduced for variant 2 at the intermediate levels as well.

The most important observation of all however is that overall, the average number of linear iterations per nonlinear iteration appears to be independent of the problem sizes for each variant

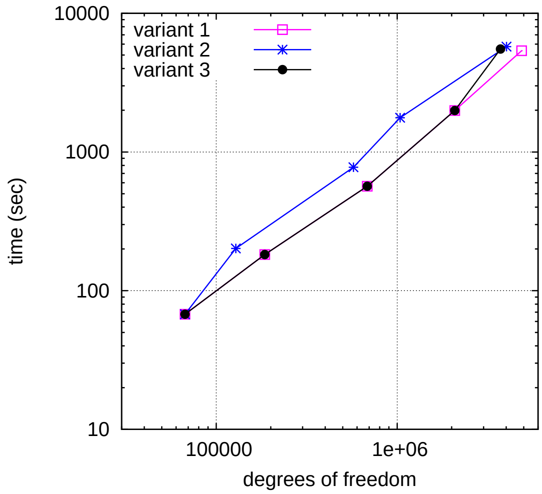

(a) $e_{tol} = 0.2e_{max}$

Figure 7: A comparison of performance of different variants of adaptive finite element solver using the finer initial mesh.

of the solver. Note that this observation provide another evidence that the performance of the preconditioner [2] is optimal within this adaptive algorithm.

As a next case, Figure 7 shows a similar behaviour in the computational times while starting with initial mesh case 2. No jump in the growth of time is observed on the first level due to the refinement of a lot more elements. Again note that the optimization of refined meshes, at least at the final level, the CPU time is the same as if the meshes are not optimized. But, the advantage of optimization of meshes is that the results thus obtained are relatively more accurate. Finally, all three variants of the solver appear to be close to optimal with approximately linear growth in the computational time (again demonstrating the optimal performance of the multilevel preconditioner). The qualitative behaviour of the iteration counts is similar to that shown in Table 3.

4.4 Further Discussion

In this subsection, an overall comparison between the behaviour and efficiency of different schemes is presented. Note that all cases presented here make use of AMG preconditioning of the elasticity block (and that geometric multigrid preconditioning is not possible for the variants of the algorithm that include the mesh optimization). Figure 8 shows a comparison of the estimated global error with respect to the computational time for the different schemes considered, using the initial mesh case 1. The hand-tuned mesh cases [3] are also included to make a comprehensive overall comparison. It can be seen that the hand-tuned mesh cases and the different variants of the adaptive algorithm are very efficient in reducing the error compared to the uniform refinement cases. Moreover, the automatic adaptivity of the different variants of the algorithm performs just as well as the hand-tuned mesh cases. Note that each variant of the adaptive algorithm is fully automatic in optimizing the computational process. On the other hand, the meshes used in the hand-tuned mesh cases are based on a large number of experiments to obtain a desired accuracy at minimal cost. Furthermore, both the variants 2 & 3 of the adaptive algorithm are comparatively better than the variant 1 in reducing the overall error at a fixed computational cost.

4.5 Accuracy of Intermediate Solves

The results presented so far were obtained by solving the nonlinear EHL problem to full accuracy at each refinement level. However, it is generally not necessary to solve the problem too accurately at each intermediate level. In other words, it is only necessary to solve a problem to a sufficient precision to obtain a good approximation to the solution in order to direct the adaptive procedure. In this subsection, the effect of different stopping tolerances for nonlinear solves at each of the intermediate levels is discussed. It should be noted that the final level problem will always be solved to full accuracy. For this purpose, an experiment is setup using variant 3. Recall that variant 3 only performs optimization on the refined meshes at the final level. In this experiment, refinement criterion $e_{tol} = 0.25\, e_{max}$ is used. Note that, there is no specific reason for the choice of variant 3 of the solver or the refinement criterion other than to make it a typical test. A total of four refinement levels are used in this experiment, with initial mesh case 1 as a base level mesh. The results obtained for different stopping tolerances for the Newton solver are given in Table 4, in terms of the number of pressure unknowns (np), the total problem size, the nonlinear iterations (ni), the linear iterations (li) and the total solve time (excluding time for optimization at the final level), the optimization time at the final level and the global error estimation.

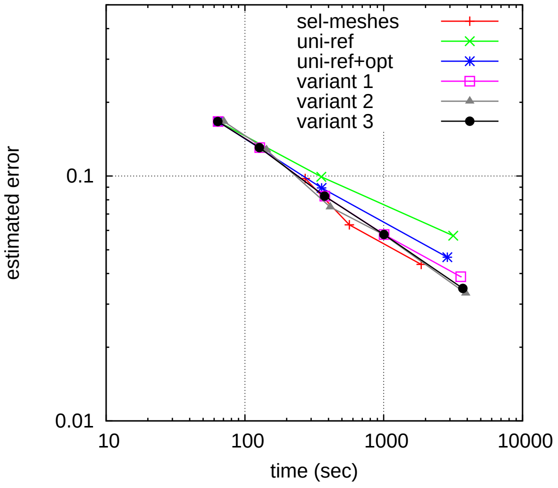

(a) $e_{tol} = 0.2 e_{max}$

Figure 8: A comparison of performance of different solvers.

Table 4: Effect of different stopping tolerances (U being the machine unit roundoff) for intermediate level nonlinear solves upon the overall performance of the adaptive solver.

abstol	np	total dof	ni	li	time (sec)	opt-time (sec)	estimated global error
$U^{\frac{1}{3}}$	12835	1569053	3	36	1640	669	0.0429396
10^{-3}	12818	1567527	3	36	1495	666	0.0429393
10^{-2}	12768	1562842	3	34	1276	666	0.0429871
10^{-1}	12747	1564912	3	32	1262	669	0.0429649
10^{-0}	12323	1277703	5	61	1327	537	0.0461213

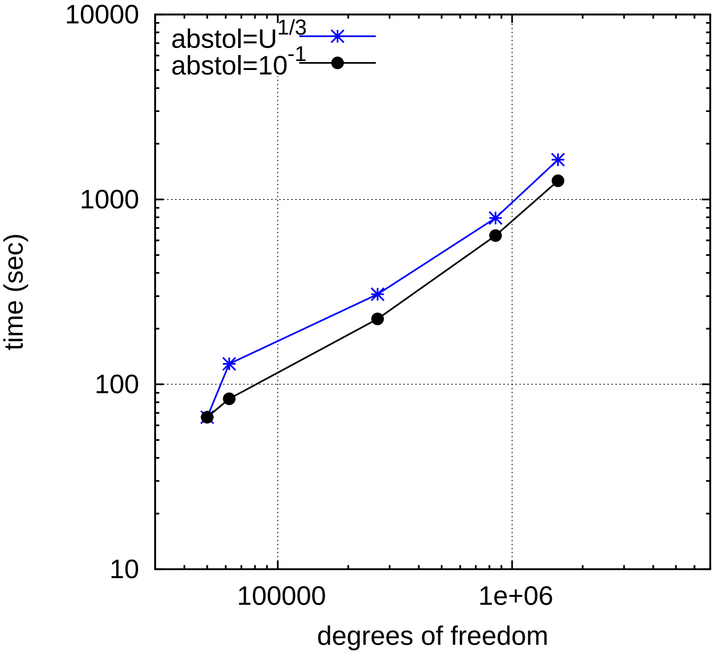

Figure 9: The effect of tolerance for the intermediate solves over the performance of an adaptive procedure.

Note that significant savings in the computational times are achieved with an increase in the tolerance. The use of tolerance as high as 10^{-1} leads to about 25% savings in the total solve time while keeping the other values almost unchanged. A further increase in the tolerance to 10^{-0} affects the refinement process more significantly. This tolerance results in a smaller problem with a relatively large error. Most probably, the quality of initial guess is also not so good causing the computational work to grow slightly compared to the 10^{-1} case. Hence, an intermediate tolerance of 10^{-1} is recommended on the basis of this, and similar, tests.

Finally, Figure 9 shows the behaviour in the growth of the computational time for the accurate and approximate solves at intermediate levels (excluding the optimization time). One can see that the jump in the computational time at the first level has not appeared in the case of the approximate solve, and the algorithm has led to a smooth linear growth in the computational time. Note that for each level i ($i = 1, 2, 3, 4$), the problem is solved approximately until the

$(i-1)^{\mathrm{th}}$ level.

5 HEAVILY LOADED PROBLEMS

So far, the accuracy and the performance of adaptive algorithm (all three variants) has been discussed in detail for a single moderately-loaded EHL case. The same overall performance of the adaptive algorithm is observed for other moderately-loaded EHL test cases, for example, the case $M = 50,\ L = 10$ with $p_h = 0.79$ G Pa [40] and the case $M = 200,\ L = 10$ with $p_h = 0.97$ G Pa [42], so they are not repeated here.

Heavily-loaded cases are comparatively more difficult to solve however. Some heavily-loaded cases may require under-relaxation as well as a better initial guess for the Newton procedure to achieve convergence. Note that throughout the work presented here no under-relaxation was used, i.e. a full Newton step was employed in the Newton procedure. However, in order to obtain a good performance of the adaptive procedure for more heavily-loaded cases one needs to provide a high quality initial guess to the next refinement level. For example, if the refined mesh following an adaptive step is not sufficiently fine then the solution of the linear elasticity equation (with interpolated pressure as traction boundary conditions) yields a better initial guess compared to an interpolated linear elastic solution. However, once the mesh is sufficiently fine then the interpolated linear elastic solution provides a slightly better initial guess. Moreover, for heavily-loaded EHL cases the fluid equation is advection-dominated in the contact region. Hence starting with a very coarse initial mesh can lead to intermediate solutions with oscillatory pressure and may even cause failure of convergence of the Newton iteration. Note that the overall stability of pressure solution is ensured with the use of SUPG method as described in [45] and addition of smoothing diffusion [22] based upon the minimum of element size in a mesh.

In the following subsections, accuracy and performance of proposed adaptive algorithm is discussed for a heavily-loaded case with $M = 1007.6,\ L = 12.05$ and $p_h = 2.0$ G Pa [41]. Based upon the performances of different variants of the adaptive algorithm as seen in the previous section, we shall only consider the variant 2 to assess the performance of adaptive algorithm. This choice provides similar accuracy to variant 3 but with lower overall memory requirements.

5.1 Accuracy

In this subsection, the accuracy appraisal of variant 2 of the adaptive solver is considered. The initial mesh is chosen sufficiently fine in order to obtain an acceptable starting solution. Table 5 shows a comparison against results from [41] in terms of central and minimum film thicknesses of the solution. It is possible to see the convergence behaviour of both of the solution methods (our adaptive algorithm and method of [41]). Note that the adaptive algorithm only targets specific regions for refinement, based upon the error estimator, so the pressure degrees of freedom are not increasing at the same rate as in Venner's model [41]. One can see that as the refinement

Table 5: Validation of results of variant 2 (with $c = 0.3$) of adaptive finite element solver: $M = 1007.6,\ L = 12.05$ and $p_h = 2.0$ G Pa.

	Venner [41]		This model			
$n_x \times n_y$	H_c	H_m	n_p	Total dof	H_c	H_m
65×65	1.213×10^{-2}	7.918×10^{-4}	–	–	–	–
129×129	2.281×10^{-2}	6.566×10^{-3}	4854	666160	2.293×10^{-2}	3.903×10^{-3}
257×257	2.613×10^{-2}	8.975×10^{-3}	6419	745902	2.453×10^{-2}	7.718×10^{-3}
513×513	2.690×10^{-2}	9.424×10^{-3}	13711	1602287	2.583×10^{-2}	8.319×10^{-3}
1025×1025	2.712×10^{-2}	9.594×10^{-3}	22154	3350526	2.656×10^{-2}	8.954×10^{-3}

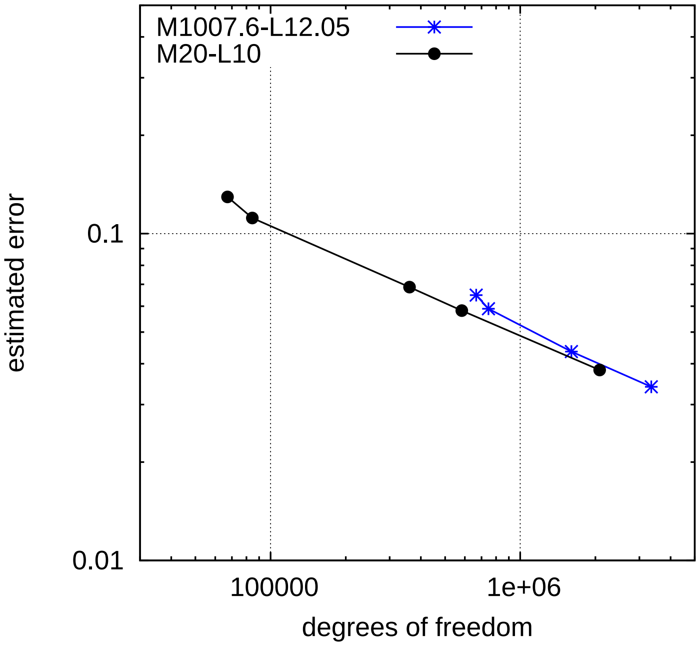

Figure 10: A comparison of global error estimation for moderately and heavily-loaded EHL cases.

level goes up both models appear to be converging to the same solution. Moreover, the difference between the solution of two models is getting smaller as the number of refinement level grows. Note that a further refinement level would require more memory than is available on a typical workstation for this 3D model. However, the results presented here still validate the accuracy of the proposed algorithm for this heavily-loaded problem (and demonstrate that adaptivity permits an equivalent accuracy to the method of [41] to be reached with far fewer degrees of freedom).

Figure 10 shows a comparison of global error estimation with respect to problem size for the moderately-loaded case ($M = 20,\ L = 10$) and heavily-loaded case ($M = 1007.6,\ L = 12.05$). It can be seen that the estimated global error for both EHL cases is reducing at the same rate with respect to problem size despite the use of different base level meshes and the additional challenges posed by the highly-loaded case. In other words, the adaptive solver for heavily-

Table 6: Statistics of solution at different refinement levels of variant 2 (with $c = 0.3$) of adaptive finite element solver: $M = 1007.6,\ L = 12.05$ and $p_h = 2.0$ G Pa.

np	total dof	ni	avg.li	time (sec)
4854	666160	15	35	1382
6419	745902	7	46	2618
13711	1602287	4	27	4533
22154	3350526	4	28	8838

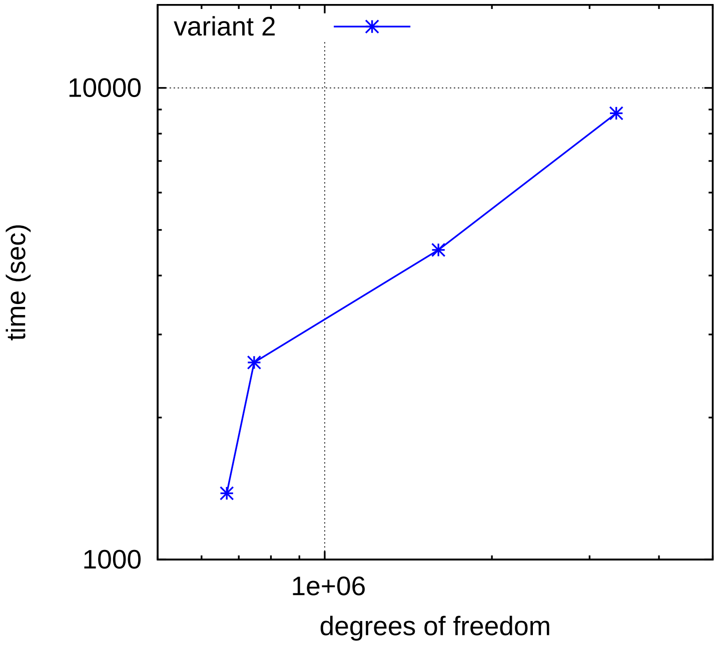

Figure 11: Performance of variant 2 (with $c = 0.3$) of adaptive finite element solver.

loaded EHL cases seems to be as effective as for the moderately-loaded EHL cases.

5.2 Performance

In this subsection, the CPU timing performance of variant 2 of the proposed adaptive finite element solver is assessed. Table 6 gives statistics for the number of nonlinear iterations, the average number of linear iterations per nonlinear iteration, and computational times for variant 2 of the adaptive solver. Note that as the refinement level goes up, the availability of the good initial guess based upon solution at the previous level leads to fewer nonlinear iterations to achieve convergence. It should be noted that for this heavily-loaded case the preconditioned iterative solver requires slightly more linear iterations per nonlinear iteration (as expected). However, the average number of linear iterations per nonlinear iteration is still independent of the problem sizes. Moreover, the computational times are growing linearly as the problem size increases, i.e. the solver still has optimal computational complexity.

Note that, for sake of demonstration, the problem is solved accurately at each refinement level to observe the performance of the preconditioned iterative solver [2] within the adaptive solver. The behaviour of the computational time with respect to problem size can be seen more clearly in Figure 11. Note that the jump in the graph after the first refinement level is similar to that in Figure 6 and may be removed by using an approximate solve at the intermediate levels (as in Figure 9). Furthermore, despite of solving the problem accurately at intermediate levels, no further jumps in the computational times are observed at later refinement levels, and the computational time grows linearly with respect to the problem size. In other words, the optimality of the preconditioned iterative solver [2] is still maintained with this adaptive algorithm for this heavily-loaded EHL case.

6 CONCLUSION

In this paper, an adaptive finite element solution to a fully-coupled EHL problem has been discussed. A ZZ-error estimator has been used to find the local and global approximations to the stress errors. These error estimations have been used to mark elements for refinement which were exhibiting larger errors than a prescribed tolerance. The local refinement of the meshes was carried out using the algorithm that is described in Section 3.3, three variants of which have been considered. The first variant applies a standard h-adaptive algorithm. The second variant considered the post-optimization of the meshes at each refinement level in order to increase the accuracy. With the post-optimization process for the meshes, a new mesh was obtained at each level which means that the hierarchy of meshes does not exist anymore. Thus, neither the derefinement nor the use of GMG based preconditioner is easily possible. Variant 3 of the adaptive solver only utilizes mesh optimization at the final level in order to avoid the possibility of excessive green elements on the 2D surface mesh (which remains unchanged by the optimization process).

The accuracy appraisal of all three variants of the solver were made using two different initial meshes against the use of uniformly refined meshes (both optimized and non optimized) and against the hand-tuned meshes [3]. The results showed that both the variant 2 and the variant 3 perform best in terms of accuracy. In other words, variant 2 & 3 have close resemblance with an hr-adaptive algorithm (at least at the final level) resulting in superior results. Although optimization of the meshes results in a loss of the nested grid property, the unchanged surface meshes allowed us to generate a high quality initial guess (by solving a linear elasticity problem with the interpolated boundary condition) to reduce the computational work at the subsequent levels. Moreover, all three variants of the solver show essentially linear growth in their computational time. Significantly, it is shown that an approximate solve at each of the intermediate levels leads to a slower linear growth in the computational time.

Furthermore, due to additional time required for the optimization process of meshes, variants 2

& 3 require a slightly longer time than the variant 1 (for a fixed problem size). However, both the variants 2 & 3 of adaptive algorithm are comparatively better than the variant 1 in reducing the overall error at a fixed computational cost. Indeed, it is demonstrated that the performance of proposed adaptive algorithm is maintained for heavily-loaded EHL cases, with the optimality of the preconditioned iterative solver [2] being preserved despite a slight increase in the solution times.

Perhaps the most important observation is that our computational experiments clearly demonstrate that using the error in the stress to control the mesh adaptivity is appropriate for fully-coupled EHL problems. The resulting adaptation of the surface mesh in the contact region allows the pressure profile to be captured accurately and with many fewer degrees of freedom than is possible with a conventional finite difference scheme. Moreover, since stress information can not be obtained using a surface integral solver based upon a half-space approximation, this adaptive approach can only be applied when a finite element approximation to the linear elasticity problem is used.

The key contributions of this work may be summarised as follows. We have introduced a new adaptive procedure for the fully-coupled EHL problem, based solely upon a local error estimate for the stress due to the elastic deformation, and demonstrated that this provides a robust mechanism for adapting the mesh in both the elasticity and the Reynolds discretizations. We have developed an adaptive strategy that combines h-refinement and r-refinement (node movement) in a manner that allows locally optimal mesh refinement. The combination of local adaptivity and our novel multigrid-based preconditioner, for the inner iterations of the Newton-Krylov solver, allow this fully-coupled EHL problem to be solved with linear time complexity for the first time: hence providing the first demonstration of the competitiveness of the fully-coupled approach with less general, but also optimal, half-space approximations such as [42]. Finally, and importantly, we have shown that the proposed technique is robust for heavily-loaded cases, which are by far the most computationally challenging.

ACKNOWLEDGEMENTS

The first author thanks to Hazara University and Higher Education Commission (HEC), Pakistan for their financial support that has allowed this research to be undertaken at the University of Leeds.

References

[1] S. Ahmed. *Efficient Finite Element Simulation of Full-System Elastohydrodynamic Lubrication Problems*. PhD thesis, University of Leeds, Leeds, UK, 2012.

[2] S. Ahmed, C. E. Goodyer, and P. K. Jimack. An efficient preconditioned iterative solution of fully-coupled elastohydrodynamic lubrication problems. *Applied Numerical Mathematics*, 62(5):649–663, 2012.

[3] S. Ahmed, C. E. Goodyer, and P. K. Jimack. On the linear finite element analysis of fully-coupled point contact elastohydrodynamic lubrication problems. *Proceedings of the Institution of Mechanical Engineers, Part J: Journal of Engineering Tribology*, 226(5):350–361, (2012).

[4] M. Ainsworth and J. T. Oden. *A posteriori error estimation in finite analysis*. John Wiley & Sons, Inc., New York, 2000.

[5] M. Ainsworth, J. Z. Zhu, A. W. Craig, and O. C. Zienkiewicz. Analysis of the Zienkiewicz-Zhu a-posteriori error estimator in the finite element method. *International Journal for Numerical Methods in Engineering*, 28:2161–2174, 1989.

[6] T. Apel, S. Grosman, P. K. Jimack, and A. Meyer. A New Methodology for Anisotropic Mesh Refinement Based Upon Error Gradients. *Applied Numerical Mathematics*, 50:329–341, 2004.

[7] I. Babuska, T. Strouboulis, C. S. Upadhyay, S. K. Gangaraj, and K. Copps. Validation of a posteriori error estimators by numerical approach. *International Journal for Numerical Methods in Engineering*, 37:1073–1123, 1994.

[8] J. Boyle, M. Mihajlovic, and J. Scott. Hsl_mi20: An efficient amg preconditioner for finite element problems in 3d. *International Journal for Numerical Methods in Engineering*, 82(1):64–98, 2010.

[9] A. Brandt and A. A. Lubrecht. Multilevel Matrix Multiplication and Fast Solution of Integral Equations. *Journal of Computational Physics*, 90(2):348–370, 1990.

[10] W. L. Briggs, V. E. Henson, and S. F. McCormick. *A Multigrid Tutorial*. Society for Industrial and Applied Mathematics, 2000.

[11] A. N. Brooks and T. J. R. Hughes. Streamline-upwind/petrov-galerkin formulations for convective dominated flows with particular emphasis on the incompressible navier-stokes equations. *Comp. Meth. Appl. Mech. Engnrg*, Vol. 32:pp.199–259, 1982.

[12] T. A. Davis. Algorithm 832: Umfpack, an unsymmetric-pattern multifrontal method. *ACM Transactions on Mathematical Software*, 30(2):196–199, June 2004.

[13] D. Dowson and G. R. Higginson. *Elastohydrodynamic Lubrication*. Pergamon Press, Oxford, 1977.

[14] H. G. Elrod. A Cavitation Algorithm. *Journal of Lubrication Technology-Transactions of the ASME*, 103:350–354, 1981.

[15] H. P. Evans and T. G. Hughes. Evaluation of Deflection in Semi-Infinite Bodies by a Differential Method. *Proceedings of the Institution of Mechanical Engineers, Part C: Journal of Mechanical Engineering*, 214:563–584, 2000.

[16] L. Floberg. *Cavitation in Lubricating Oil Films*. Elsevier, Amsterdam, 1964.

[17] C. E. Goodyer. *Adaptive Numerical Methods for Elastohydrodynamic Lubrication*. PhD thesis, University of Leeds, Leeds, UK, 2001.

[18] C. E. Goodyer and M. Berzins. Adaptive timestepping for elastohydrodynamic lubrication solvers. *SIAM Journal on Scientific Computing*, 28:626–650, 2006.

[19] C. E. Goodyer and M. Berzins. Parallelization and scalability issues of a multilevel elastohydrodynamic lubrication solver. *Concurrency and Computation: Practice and Experience*, 19:369–396, 2007.

[20] W. Habchi. *A Full-System Finite Element Approach to Elastohydrodynamic Lubrication Problem: Application to Ultra-Low-Viscosity Fluids*. PhD thesis, University of Lyon, France, 2008.

[21] W. Habchi, D. Eyheramendy, P. Vergne, and G. Morales-Espejel. A full-system approach of the elastohydrodynamic line/point contact problem. *ASME Journal of Tribology*, 130(2), 2008.

[22] W. Habchi, D. Eyheramendy, P. Vergne, and G. Morales-Espejel. Stabilized Fully-Coupled Finite Elements for elastohydrodynamic Lubrication Problems. *Advances in Engineering Software*, 46(1):4–18, 2012.

[23] M. J. A. Holmes, H. P. Evans, T. G. Hughes, and R. W. Snidle. Transient Elastohydrodynamic Point Contact Analysis Using a New Coupled Differential Deflection Method. Part I: Theory and Validation. *Proceedings of the Institution of Mechanical Engineers, Part J: Journal of Engineering Tribology*, 217:289–303, 2003.

[24] M. J. A. Holmes, H. P. Evans, T. G. Hughes, and R. W. Snidle. Transient Elastohydrodynamic Point Contact Analysis Using a New Coupled Differential Deflection Method. Part II: Results. *Proceedings of the Institution of Mechanical Engineers, Part J: Journal of Engineering Tribology*, 217:305–321, 2003.

[25] L. G. Houpert and B.J. Hamrock. Fast approach for calculating film thicknesses and pressures in elastohydrodynamically lubricated contacts at high loads. *ASME Journal of Tribology*, Vol 108:pp. 411–420, 1986.

[26] T. G. Hughes, C. D. Elcoate, and H. P. Evans. Coupled Solution of the Elastohydrodynamic Line Contact Problem Using a Differential Deflection Method. *Proceedings of the Institution of Mechanical Engineers, Part C: Journal of Mechanical Engineering*, 214:585–598, 2000.

[27] R. Lohner and J. D. Baum. Adaptive h-refinement on 3d unstructured grids for transient problems. *International Journal for Numerical Methods in Fluids*, 14:1407–1419, 1992.

[28] H. Lu. *High Order Finite Element Solution of Elastohydrodynamic Lubrication Problems*. PhD thesis, University of Leeds, Leeds, UK, 2006.

[29] A. A. Lubrecht. *Numerical solution of the EHL line and point contact problem using multigrid techniques*. Phd thesis, University of Twente, Endschende, The Netherlands, 1987.

[30] R. Mahmood and P. K. Jimack. Locally optimal unstructured finite element meshes in 3 dimensions. *Computers and Structures*, 82:2105–2116, 2004.

[31] J. E. Marsden and T. J. R. Hughes. *Mathematical Foundations of Elasticity*. Dover Publications, Inc., New York, 1994.

[32] M. Moller and D. Kuzmin. Adaptive mesh refinement for high-resolution finite element schemes. *International Journal for Numerical Methods in Fluids*, 52(5):545–569, 2006.

[33] K. P. Oh and S. M. Rohde. Numerical solution of the point contact problem using the finite element method. *International Journal for Numerical Methods in Engineering*, Vol 11:pp. 1507–1518, 1977.

[34] H. Okamura. A contribution to the numerical analysis of isothermal elastohydrodynamic lubrication. *Proc. 9th Leeds-Lyon Symp. Trib.*, 1982(Leeds, UK).

[35] C. J. A. Roelands. *Correlational Aspects of the Viscosity-Temperature-Pressure Relationship of Lubricating Oils*. PhD thesis, Technische Hogeschool Delft, The Netherlands, 1966.

[36] Y. Saad and M. H. Schultz. Gmres: a generalized minimal residual algorithm for solving nonsymmetric linear systems. *SIAM Journal on Scientific and Statistical Computing*, 7:856–869, 1986.

[37] J. Schoeberl. Netgen, an advancing front 2d/3d-mesh generator based on abstract rules. *Comput. Visual. Sci.*, 1:41–52, 1997.

[38] W. Speares and M. Berzins. A 3d unstructured mesh adaptation algorithm for time-dependent shock-dominated problems. *International Journal for Numerical Methods in Fluids*, 25(1):81–104, 1997.

[39] U. Trottenberg, C. W. Oosterlee, and A. Schuller. *Multigrid*. Academic Press, 2001.

[40] C. H. Venner and J. Bos. Effects of lubricant compressibility on the film thickness in EHL line and circular contacts. *Wear*, 173:151–165, 1994.

[41] C. H. Venner and A. A. Lubrecht. Multigrid techniques: A fast and efficient method for the numerical simulation of elastohydrodynamically lubricated point contact problems. *Proceedings of the Institution of Mechanical Engineers, Part J: Journal of Engineering Tribology*, 214:43–62, 2000.

[42] C. H. Venner and A. A. Lubrecht. *Multilevel Methods in Lubrication*. Elsevier, Netherlands, 2000.

[43] C.H. Venner. *Multilevel Solution of the EHL Line and Point Contact Problems*. Phd thesis, University of Twente, Endschende, The Netherlands, 1991.

[44] S. R. Wu. A penalty formulation and numerical approximation of the reynolds-hertz problem of elastohydrodynamic lubrication. *International Journal of Engineering Science*, Vol. 24(No.6):1001–1013, 1986.

[45] O. C. Zienkiewicz and R. L. Taylor. *The Finite Element Method, 5th edition, Volume 3: Fluid Dynamics*. Butterworth-Heinmann, Oxford, 2000.

[46] O. C. Zienkiewicz, R. L. Taylor, and J. Z. Zhu. *The Finite Element Method: Its Basis and Fundamentals, Sixth Edition*. Elsevier Butterworth-Heinemann, 2005.

[47] O. C. Zienkiewicz and J. Z. Zhu. A simple error estimator and adaptive procedure for practical engineering analysis. *International Journal for Numerical Methods in Engineering*, 24(2):337–357, 1987.

[48] O. C. Zienkiewicz and J. Z. Zhu. The superconvergence patch recovery and a posteriori error estimates. Part 1: The recovery techniques. *International Journal for Numerical Methods in Engineering*, 33:1331–1364, 1992.

[49] O. C. Zienkiewicz and J. Z. Zhu. The superconvergent patch recovery and a posteriori error estimates. Part 2: Error estimates and adaptivity. *International Journal for Numerical Methods in Engineering*, 33:1365–1382, 1992.